[Digitare il testo]

PERFORMANCE ASSESSMENT OF ADIABATIC COMPRESSED AIR ENERGY STORAGE (A-CAES) POWER PLANTS INTEGRATED WITH PACKED-BED THERMOCLINE STORAGE SYSTEMS

Vittorio Tola, Valentina Meloni, Fabrizio Spadaccini, Giorgio Cau
University of Cagliari, Department of Mechanical, Chemical and Materials Engineering
Via Marengo 2, 09123 Cagliari, Italy,
Tel. ++39 070 6755102, e-mail: vittorio.tola@dimcm.unica.it

ABSTRACT

Among energy storage technologies, compressed air energy storage (CAES) systems have undergone a real development since the 70s, although only two large-size commercial plants are operating worldwide. CAES systems allow very large energy storage to be performed, accumulating compressed air to be used for electrical energy generation. In recent years, A-CAES (Adiabatic Compressed Air Energy Storage) plants have had an important role. This technology allows the storage of the thermal energy released during air compression to be used for heating the compressed air during electricity generation, avoiding the consumption of fossil fuels.

The main objective of this paper is to propose an innovative system solution for large-size A-CAES plants. The proposed configuration is characterized by: i) a compression train based on two axial compressors constantly operating at design conditions and a centrifugal compressor fully devoted to managing the pressure variation, ii) a thermocline thermal energy storage (TES) system based on a packed bed of solid material located between the low-pressure and high-pressure compressors, iii) an expansion train based on a high-pressure radial turbine and a low-pressure axial turbine.

TES performance was evaluated with integration with the A-CAES plant through a dedicated numerical simulation model. Operating modes for managing the high-pressure and low-pressure turbines through air throttling and high-pressure turbine bypassing were also studied. Finally, an in-depth analysis of the off-design behaviour of the different A-CAES components was carried out. Globally the A-CAES round trip efficiency exceeds 0.7–0.75.

Keywords: Compressed Air Energy Storage, A-CAES, Thermal Energy Storage, Thermocline, CAES Machinery

NOMENCLATURE

C	heat capacity
E	energy
h_{SF}	convective heat transfer coefficient
k_{eff}	effective conductivity
m	mass
M	motor
t	time
T	temperature
u	velocity
x	distance along the axial direction

Greek symbols

α_{SR}	specific surface area
β	pressure ratio

45	ΔP	pressure losses
46	ε	void fraction
47	η	efficiency
48	ρ	density
49		
50	*Subscripts*	
51	f	fluid
52	F	fuel
53	is	isentropic
54	M	compressor
55	p	pressure
56	ref	reference
57	RT	round trip
58	s	solid
59	T	turbine
60	v	volumetric
61		
62	*Acronyms*	
63	AA-CAES	Advanced Adiabatic Compressed Air Energy Storage
64	A-CAES	Adiabatic Compressed Air Energy Storage
65	AC	AfterCooler
66	AR	Aspect Ratio
67	CAES	Compressed Air Energy Storage
68	D-CAES	Diabatic Compressed Air Energy Storage
69	DGV	Diffuser Guide Vane
70	DIMCM	Department of Mechanical Chemical and Materials Engineering
71	HP	High Pressure
72	HPC	High Pressure Compressor
73	HPT	High Pressure Turbine
74	I-CAES	Isothermal Compressed Air Energy Storage
75	IC	InterCooler
76	IPC	Intermediate Pressure Compressor
77	ISEP	Iowa Stored Energy Park
78	LP	Low Pressure
79	LPC	Low Pressure Compressor
80	LPT	Low Pressure Turbine
81	LTA-CAES	Low Temperature Adiabatic Compressed Air Energy Storage
82	O-CAES	Ocean Compressed Air Energy Storage
83	RES	Renewable Energy Sources
84	RPM	Revolutions per Minute
85	SOC	State Of Charge
86	TES	Thermal Energy Storage
87	TIT	Turbine Inlet Temperature
88		
89		

90 ## 1. INTRODUCTION

91   The worldwide production of electricity from renewable energy sources (RES), wind and solar in particular, has
92 grown significantly in the last decade and it is expected to keep up a strong growth trend in the near future [1]. Non-hydro
93 RES contributed 6% to the worldwide electricity generation in 2014 and their contribution is expected to range between
94 12 and 18% in 2025, depending on the policy scenario considered [1]. On the other hand, the non-programmable character

95 of solar and wind energy sources, due to their intermittent and fluctuating behaviour, calls for a significant diffusion of
96 energy storage technologies to improve the flexibility and efficiency of energy systems and the usability of non-
97 programmable energy sources [2–4].
98   In this contest a key role can be played by energy storage systems. Such systems allow to store electrical energy by
99 converting it to a different form of energy (chemical, mechanical, electrostatic or electromagnetic) [2]. The storage
100 systems allows to temporally decouple production and consumption of electricity ensuring a reserve to couple with
101 unpredictable power peaks. Storage systems also have an essential role in isolated systems, allowing supply continuity in
102 periods of lost production, as in the case of photovoltaic systems during cloudy and night hours [5]. As a matter of fact,
103 storage systems can occupy a major role in electricity grids based on renewable sources [3].
104   Different energy storage technologies are available today and in continuous development [4,6]. The most widespread
105 are pumped hydroelectric plants and electrochemical accumulators, such as solid state and flow batteries. Worldwide, the
106 energy storage systems currently account for an installed capacity of about 130 GW and more than 99% is ascribed to
107 pumped hydroelectric plants [7]. Among storage technologies, the compressed air energy storage systems, commonly
108 known by the acronym CAES, are among the most promising technologies for large capacity energy storage systems [8].
109 CAES systems have undergone a real development since the 70s, although only two large-size commercial plants are
110 currently operating worldwide (Huntorf [9] and McIntosh [10]). The CAES technology exploits the possibility of
111 accumulating large amounts of energy as compressed air during low electrical load demand periods, with low specific
112 investment costs. As pumped-hydro, CAES plants are the sole storage plants capable of providing an amount of energy
113 comparable to large power plants for electrical energy production [8], with a theoretical power capacity up to thousands of
114 MW.
115   A CAES system is composed of an electrically driven compressor, a compressed air storage system, a gas turbine, an
116 electric motor/generator and a compressed air heating system. The compressed air is stored in a reservoir (usually an
117 underground cavern, a deep aquifer or another suitable structure) at a pressure which typically varies between 40 and 100
118 bar. The energy production phase consists in the release of the compressed air from the cavern, the air heating (via a
119 regenerative heat exchanger and/or a combustion chamber) and the expansion in a conventional gas turbine [8].
120   Over the years, different plant arrangements have been proposed for CAES plants, differing in performance and
121 complexity. The conventional diabatic CAES (D-CAES) is composed of a series of electrically driven chilled
122 compressors, a reservoir for air storage, a combustion chamber, one or more expanders and an electric generator. This
123 arrangement, however, does not consider the recovery of the thermal energy released during compression intercooling. In
124 a more advanced D-CAES arrangement, the pressurized air from the reservoir is preheated in a regenerative heat
125 exchanger, exploiting the thermal energy of the gas turbine exhaust.
126   The existing commercial plants and many of the plants under construction and/or in the planning phase are based on
127 conventional D-CAES, but various technological improvements could be pursued to enhance the performance and reduce
128 the costs and environmental impact of CAES systems. The most interesting and widely studied opportunity for
129 improvement is to eliminate the use of fuel, and consequently the related CO_2 emissions, by performing a thermal energy
130 recovery and introducing a thermal energy storage (TES) system [11–13]. In such a system, commonly known as adiabatic
131 CAES (A-CAES), the heat recovery can be performed in some or in all the stages of the compression phase. The stored
132 heat can thus be exploited later, during the generation phase, to heat the compressed air coming from the reservoir without
133 using any fuel. The TES systems can be based on thermal oil [14], phase change materials [15] or solid materials [16].
134 Although heat recovery leads to performance improvements, the process involves some technological, thermodynamic
135 and operational issues, including the off-design behaviour of system components and the choice of both storage
136 technology and materials.
137   The growing interest in CAES as an effective solution to manage non-dispatchable energy sources has led in recent
138 years to a multiplication of the research activities in this sector. In particular, at the end of the last decade Lund et al.
139 studied the strategy of integration of CAES systems with sustainable energy systems based on RES [17]. Lund et al.
140 concluded that CAES technologies can be used for electricity balancing in future energy systems with a high share of
141 intermittent and fluctuating RES [18]. In particular, CAES plants will often operate on electricity spot markets by storing
142 energy when electricity prices are low and producing electricity when prices are high. Several papers analyze A-CAES
143 plants with particular attention to the integration with RES. Arabkoohsar et al. [19,20] and Zafirakis et al. [21] studied the
144 integration of A-CAES and PV plants. In particular, Arabkoohsar et al. studied both the integration of a CAES unit with an
145 ancillary solar heating system for a large scale PV farm [19] and the feasibility of employing a city gas station power

146 output for improving the performance of a grid connected PV plant accompanied with a CAES system and enhancing its
147 power output stability [20]. Zafirakis et al. developed an algorithm for sizing photovoltaic based compressed air energy
148 storage systems. More studies analyze the integration with wind power, such as Zunft et al. [22], who showed the
149 technical feasibility of the concept and good prospects for its economical viability and Zhao et al. [14,23], who designed a
150 hybrid system based on A-CAES, flywheel and wind power. Other papers evaluate the influence of TES systems, mainly
151 considering indirect contact heat exchangers. Grazzini and Milazzo discussed design criteria [24], Hartmann et al.
152 analyzed different A-CAES configurations [25], Barbour et al. suggested packed bed thermal energy storage systems [16],
153 Wolf and Budt introduced a low temperature adiabatic CAES (LTA-CAES) plant [26] concluding that the faster start-up
154 and wide-ranging part load ability of the LTA-CAES compensate for the lower round trip efficiency compared to high
155 temperature A-CAES. Minutillo et al. [27] analyze the performance of small-size A-CAES, that, integrated with a PV
156 system, supplies electric power to a small scale off-grid base transceiver station. Manfrida and Secchi [28] integrated a
157 small-size A-CAES with a CHP solution, where the heat recovered from compressor cooling is used for heating purposes,
158 while Garrison and Webber proposed a hybrid A-CAES that uses solar energy to heat the HP air from a cavern before
159 expansion [29].
160   On the other hand, to the best knowledge of the authors, in the literature there is a shortage of studies concerning, in
161 particular, the off-design behaviour of the plant components. This work reports an in-depth study of an A-CAES plant
162 integrated with a TES system based on the thermocline principle in a packed-bed of bulk solid material, proposing a novel
163 A-CAES configuration and operation mode. In particular, the main novelty and contributions of this work involve:

164   1. the proposal of a novel A-CAES configuration. The proposed configuration is characterized by: i) a
165   compression train based on two axial compressors constantly operating at design conditions and a centrifugal
166   compressor fully devoted to managing the pressure variation, ii) a thermocline TES system based on a packed
167   bed of solid material located between the low-pressure and high-pressure compressors, iii) an expansion train
168   based on a high-pressure radial turbine and a low-pressure axial turbine;
169   2. the development of a numerical simulation model of the TES system and the evaluation of the TES
170   performance when integrated with the A-CAES plant;
171   3. the study of two operating modes for managing the high-pressure and low-pressure turbines through air
172   throttling and high-pressure turbine bypassing;
173   4. the in-depth analysis of the off-design behaviour of the A-CAES plant components.

2. A brief overview on CAES plants

2.1 CAES configurations

177   Over the years, different plant arrangements have been proposed for CAES plants, differing in performance and
178 complexity. Nowadays, different concepts of CAES systems can be identified. In particular, in addition to the
179 conventional diabatic CAES, the most interesting configurations are adiabatic and isothermal CAES plants. The
180 classification criteria derive from heat handling during the compression and expansion phases. As previously specified,
181 the conventional diabatic CAES involves the dissipation of thermal energy during air compression. More advanced D-
182 CAES solutions include a regenerative heat exchanger for preheating the pressurized air exiting the reservoir by recycling
183 heat recovered by the gas turbine exhaust. A more significant improvement can be achieved through the A-CAES plants,
184 where the heat recovered by the compression is accumulated on a TES system for the deferred heating of the pressurized
185 air, without using any fuel, during the generation phase. In this case, the turbine inlet temperature, and therefore the
186 maximum compression and storage temperature, must be high enough to achieve adequate system performance.
187 Consequently, the main aim of R&D programs on Advanced A-CAES is to find innovative solutions for compressor
188 operating temperatures up to 600 °C, or even up to 700 °C, taking into account the cyclic system operation and pursuing
189 high efficiencies also at part-load conditions [30]. The isothermal CAES (I-CAES) technology has been developed more
190 recently [31]. Several companies are developing small-scale prototypes applying reciprocating piston machinery for air
191 compression and expansion [32]. The air temperature is kept low by directly injecting water spray into the compression
192 chamber [8]. Nowadays, research on I-CAES mainly focuses on the development of machines that allow compression and
193 expansion processes as close as possible to isothermal conditions [33]. Other possible arrangements for CAES systems
194 have also been studied, such as the integration with combined cycles (CC). In such systems, during the CAES discharge

195 phase, a fraction of the GT exhaust mass flow is diverted to a recuperator to heat the stored compressed air before its
196 expansion in the turbine [34]. An advanced concept of CAES provides for the use of a steam injection cycle, exploiting
197 the flue gases' sensible heat to produce steam to be injected inside the combustion chamber. Another solution to increase
198 the CAES power is humidification of the preheated air [35].
199   Different solutions for the compressed air storage can also be adopted. Storage reservoirs can be placed above or
200 below ground level or also below sea level (O-CAES plants). The main underground reservoirs are rock caverns, salt
201 domes or porous media [36]. Reservoirs under the sea are typically hollow spheres or inflatable balloons [37]. Above all,
202 the integrity of these systems for several tens of years must be guaranteed, as they are subjected to daily charge-discharge
203 cycles. In fact, oxygen and bacteria have detrimental effects on rock formations, due to oxidative effects. Generally, the
204 use of pre-existing underground cavities is preferred, significantly reducing costs. As a matter of fact, it is necessary to
205 highlight that land and subsoil suitable for CAES systems are not easily available at competitive cost.
206
207   *2.2 CAES performance parameters*
208   In energy storage systems, the round trip efficiency can be defined as the ratio between the energy retrieved from
209 storage and the energy put in. In fact, conventional D-CAES is not a mere electrical energy storage technology, such as
210 electrochemical batteries, but it is also a peak generating technology [8], including a double energy input: electrical energy
211 is used for driving the compressors, while fuel provides the thermal energy required for heating air in the generation
212 phase. Consequently, for D-CAES systems the definition of energy performance is more complicated and several different
213 energy parameters for the definition of CAES efficiency have been proposed in the literature [8,38]. In particular, the
214 simplest CAES performance index defines the round trip efficiency η_{RT1} as the ratio of the electrical energy generated by
215 the turbine E_T and the sum of the electrical energy required by the compressor E_M and the fuel chemical energy E_F [8]:
216

$$\eta_{RT1} = \frac{E_T}{E_M + E_F} \qquad (1)$$

217
218   However, due to the different thermodynamic value of fuel and electrical energy, the fuel chemical energy should be
219 expressed as equivalent electrical energy, introducing a reference conversion efficiency η_{ref} referred, for example, to a
220 heavy duty gas turbine, leading to the definition of the round trip efficiency η_{RT2}:
221

$$\eta_{RT2} = \frac{E_T}{E_M + E_F \eta_{ref}} \qquad (2)$$

222
223   Obviously, in the case of adiabatic CAES, the two definitions coincide, being $E_F = 0$.
224
225   *2.3 CAES costs*
226   An accurate estimation of CAES costs is quite complicated, due to the lack of data available from existing
227 installations. Both large-size plants currently in operation present a capital cost of about 400 $/kW, but the data refer to
228 some decade ago. Moreover, CAES capital costs are strictly dependent on the technology, size and site. The literature
229 includes some data describing plant capital costs as a function of CAES size [39–41]. In particular, a capital cost in the
230 range of 400–1000 $/kW is expected for large-size CAES [39], whereas capital costs of small-size CAES are in the range
231 500–1500 [39]. The costs of storage insulation and safety depend on the specific geomorphology of the site. Costs are also
232 influenced by the storage strategy. An overly aggressive strategy, serving just the electrical peaks for a few hours a day,
233 would lead to uneconomic capital costs. Rapid extraction of the stored energy would lead to high costs for the expansion
234 train and the alternator. The best strategy from an economic point of view follows the electricity demand in a not
235 excessively speculative way.
236
237   *2.4 Existing CAES plants*

As previously mentioned, worldwide only two CAES plants are currently operating: the Huntorf plant and the McIntosh plant. Both plants are based on conventional diabatic technology (D-CAES) and are fuelled by natural gas [9,10].

The Huntorf plant has been operating since 1978 in the north of Germany. The compressed air is stored in two salt caverns located 600 m below ground level (total volume larger than 170000 m^3) and supporting a maximum pressure of 70 bar. Energy from nuclear power plants is stored at night for about 12 hours. Electrically driven compressors, intercooled without heat recovery, absorb about 60 MW. The accumulated energy is released for 3 hours, through a 320 MW gas turbine, covering peak loads. In addition, the CAES plant acts as a hot reserve for industrial customers and allows the variable energy generation from wind farms to be levelled. A throttling valve assures a constant pressure at the HP turbine inlet equal to 42 bar. The Huntorf plant shows a round trip efficiency equal to 0.42.

The McIntosh CAES plant was built in 1991 in Alabama (USA). This D-CAES plant is characterized by several improvements over the Huntorf plant, such as the regenerative heat recovery of the exhaust gas, reducing the fuel consumption by about 25%, with a round trip efficiency equal to 0.54. A salt cavern, located 500 m below ground level with a volume of over 500000 m^3, is used as reservoir, storing compressed air at a pressure between 46 and 74 bar. The McIntosh plant assures a power output of 110 MW for about 26 hours, requiring 1.7 hours of compression for each hour of generation. The plant is used as a hot reserve, to cover peak loads and for grid load levelling. The plant can handle transients in the order of 18 MW per minute, about 60% more than conventional gas turbine plants. The air is stored during night hours, pressurized through two intercooled compressors. Upstream of the HP turbine, the air is throttled to 43 bar.

Although the existing CAES plants have been operating for several decades, the technology is still in a state of development. Several projects regarding CAES plants were developed in the past or planned for the future around the world, especially in the US. In the 2000s, a project involving the construction of a 800 MW plant at Norton, Ohio was studied for over a decade with the possibility to be expanded up to 2700 MW [42]. In the middle of the 2000s, the construction of the ISEP (Iowa Stored Energy Park) plant in Iowa was planned. The plant implied the integration of a wind facility (supposed 75–150 MW power) with a 260 MW CAES plant, with an underground storage in an aquifer located at 900 m depth [43]. The project was cancelled in 2013 due to site geological limitations. The Seneca CAES project was announced by NYSEC in the Eastern US, exploiting an existing underground salt cavern. The plant was designed for a rated capacity of about 150 MW. The key objective was to improve the grid reliability by creating an electricity storage system for a more desirable dispatch of wind energy. The project was cancelled in 2012 due to economic issues [44]. Two other projects (Bethel Energy Center and Matagorda Energy Center) are planned in Texas by Apex CAES [45,46], with the aim of operating two D-CAES plants (320 and 540 MW, respectively). The Pacific Northwest National Laboratory and the Bonneville Power Administration have developed two projects on CAES systems (Columbia Hills and Yakima Minerals, respectively) to store in subterranean caverns the wind excess energy produced in the North Western US [47]. In Japan, since 1990 the Japanese New Energy Foundation has been carrying out experiments on CAES technology with the aim of evaluating the CAES performance in load levelling. The 2 MW pilot plant, located at Kamisunagawa-cho, stores compressed air (40–80 bar) in a depleted coal mine [48]. A D-CAES plant exploiting underground salt formation for storage is planned to be built at Larne, Northern Ireland [49,50]. The facility will generate up to 330 MW for 6 hours, with a 200 MW compression power request. The project involves the creation of two storage caverns within a salt deposit, which will be located at depths of 1400 m below ground level. In addition, in Europe several projects for D-CAES are in the first phases of planning in the UK, Denmark and Germany [51].

Recent studies suggest that the advanced TES technologies, together with improvements in the compressor and turbine systems, could make the CAES technology economically sustainable. Such a concept, the so-called AA-CAES (Advanced Adiabatic CAES), would achieve an efficiency of about 70%, without fuel consumption, in large-size CAES plants [52]. In this context, the ADELE project is under development in Europe [30]. The ADELE will be the third CAES plant in the world, but the first to be based on the AA-CAES technology. The plant will have a storage capacity of 360 MWh and an electric output of 90 MW [53].

3. PROPOSED A-CAES SYSTEM DESCRIPTION AND ASSUMPTIONS

288   *3.1 System description*
289
290   Figure 1 shows the simplified functional scheme of the A-CAES system proposed and assessed in this study.
291
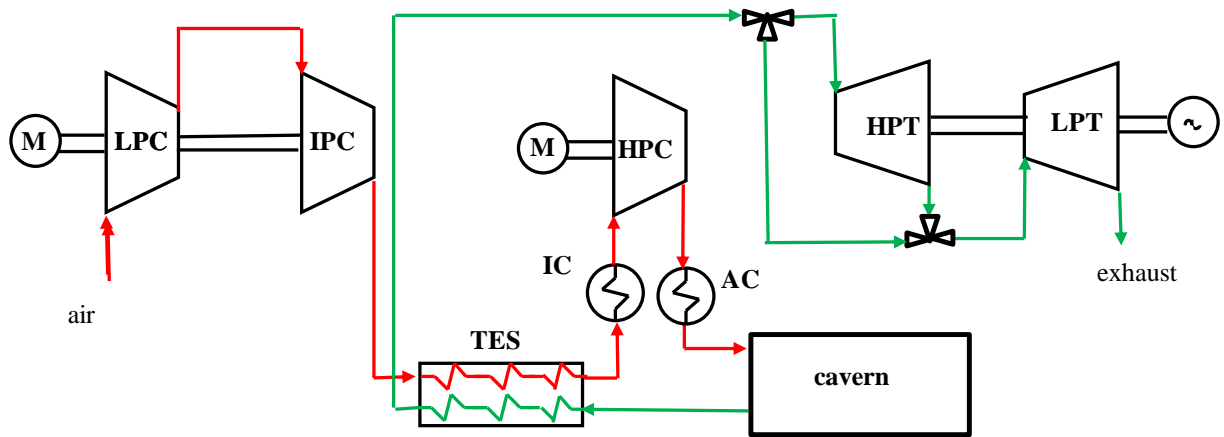
Figure 1. Simplified scheme of the A-CAES plant.

292
293   A first section of the compression system includes a low-pressure compressor (LPC) and an intermediate-pressure
294   compressor (IPC), followed by a TES system where the compressed air is cooled and its thermal energy recovered and
295   accumulated. Downstream of the TES system, a high-pressure compressor (HPC) raises the air pressure up to the
296   maximum operating pressure, corresponding to the backpressure of the reservoir (a hypothetical cavern), assumed to
297   range between 60 and 100 bar. Between the TES system and the HPC, an intercooler heat exchanger (IC) accomplishes
298   the air cooling in order to reduce the HPC power consumption. The air is then stored at high pressure in the cavern, to be
299   subsequently extracted during the discharge phase. Inasmuch as the temperature inside the cavern is limited between 30
300   and 50 °C by structural stability concerns, the air exiting the HPC is cooled in an aftercooler heat exchanger (AC). During
301   the discharge phase, the compressed air exiting the cavern is heated inside the TES system before expanding through the
302   high-pressure (HPT) and low-pressure (LPT) turbines. A portion of the high-temperature compressed air flow can bypass
303   the HPT and directly feed the LPT, in order to increase the temperature of the air entering the LPT and to avoid an exhaust
304   temperature lower than 25 °C, as a minimum reference value established in this study to avoid water condensation issues.
305   Since the compression and expansion processes take place separately, turbines and compressors are coupled to different
306   shafts.
307   Giving consideration to large-size A-CAES systems, a design power output equal to 100 MW was assumed. The A-
308   CAES system was supposed to cover daily peaks of electricity and thus a discharge phase of 3 hours was established.
309   Starting from the main turbine parameters reported in the section 3.4 with the expansion system assumptions, this power
310   output requires, at nominal conditions, a turbine air mass flow rate of about 170 kg/s. Assuming a charge phase duration
311   of 8 hours, the cavern mass balance leads to a charge air mass flow rate of about 65 kg/s. The compressor inlet pressure
312   and temperature are set equal to ambient conditions. The temperature of the compressed air entering the TES system
313   (equal to the IPC output temperature) is set to 600 °C. The air outlet temperature from the TES system in the charge phase
314   is assumed equal to 35 °C at reference design conditions and increases during operation, requiring an intercooler upstream
315   of the HPC. The HPC allows the existing backpressure in the cavern to be overcome by varying its discharge pressure
316   from 60 to 100 bar. During the subsequent 3-hour phase of power generation, the pressure in the cavern, and consequently
317   the HPT inlet pressure, vary conversely from 100 bar to 60 bar. A pressure of 1.02 bar was also considered for the exhaust
318   gases at the LPT outlet. Table 1 summarizes the main operating parameters of the A-CAES plant:
319

Table 1. Main parameters of the A-CAES plant

Power output	100 MW
Discharge time	3 h
Charge time	8 h

Discharge air mass flow	173.0 kg/s
Charge air mass flow	64.9 kg/s
Compressor train inlet temperature	15 °C
Compressor train inlet pressure	1 bar
Design TES inlet temperature in the charge phase	600 °C
Design TES outlet temperature in the charge phase	35 °C
Cavern maximum pressure	100 bar
Cavern minimum pressure	60 bar
Expansion train outlet pressure	1.02 bar

320
321   As mentioned, this study does not refer to an existing cavern and the operating pressure range (60-100 bar) was
322 assumed according to typical values for CAES systems. Starting from charge air mass flow (about 65 kg/s) and charge
323 time (8 hours), an amount of charge air of about 1870 tons was calculated. Considering the ideal gas behaviour, a cavern
324 volume larger than 40000 m^3 and an air mass at the minimum pressure amounting of about 2800 tons and were also
325 calculated. Consequently at the end of the charge phase the amount of air inside the cavern is equal to about 4700 tons.
326
327
328   *3.2 Compression system assumptions*
329
330   The first compression stage is performed by both LPC and IPC, of axial type, which make it possible to process great
331 volume flows with high efficiency. Furthermore, multistage axial compressors allow greater pressure ratios in comparison
332 to centrifugal ones, despite a lower pressure increase per stage. A pressure ratio of 13 and a polytropic efficiency of 0.92
333 were assumed for the LPC, which operates in the temperature range of typical industrial compressors. The LPC outlet
334 temperature (corresponding to the IPC inlet temperature) exceeds 375 °C, leading to unusual conditions at the IPC inlet.
335 To reach a final temperature of 600 °C at the IPC outlet, an IPC pressure ratio equal to 2.76 was required, resulting in an
336 outlet pressure equal to about 37 bar. A polytropic efficiency equal to 0.9 was set for the IPC. The LPC and IPC constantly
337 operate at design conditions, as the pressure variation for overcoming the cavern backpressure is fully managed by the
338 HPC, assuring constant temperature and pressure conditions at the inlet of the TES system.
339   For the proposed A-CAES configuration the HPC pressure ratio varies between 1.62 at the cavern minimum pressure
340 conditions (60 bar), and 2.71 at the cavern maximum pressure (100 bar). Therefore, a single-stage centrifugal compressor
341 was chosen and designed. In fact, despite a lower efficiency compared to axial compressors, centrifugal ones allow higher
342 pressure ratios per stage (up to 3–4) and are preferable in the case of a lower pressure ratio. Moreover, they are more
343 versatile and stable when operating under off-design conditions. Typically, the mass flow rate and pressure ratio of
344 centrifugal compressors are controlled by varying the stagger angle of the Diffuser Guide Vane (DGV) or the RPM
345 through an inverter. RPM variation is not economically feasible for power higher than 1 MW, therefore a variable DGV
346 was chosen to manage pressure variation. Finally, the compressor size is quite small, due to the high air inlet density
347 (about 42 kg/m^3 at 37 bar and 35 °C). Table 2 reports the main characteristics of the three compressors:
348

Table 2. Main parameters of the compressors

Compressor	LPC	IPC	HPC
Air mass flow	64.9 kg/s	64.9 kg/s	64.9 kg/s
Pressure ratio	13.0	2.81	1.62–2.71
Compressor outlet pressure	13.2 bar	37.0 bar	60–100 bar
Compressor outlet temperature	376.1 °C	600 °C	88–118 °C
Polytropic efficiency	0.92	0.90	0.683–0.908

349
350 The HPC is connected to a different shaft than the LPC and IPC, operating at a higher rotation speed.
351

352
353   *3.3 TES system assumptions*
354
355   A Thermal Energy Storage (TES) system was introduced to accumulate the thermal energy recovered by the high-
356   temperature (600 °C) air exiting the IPC. In the discharge phase, the TES system heats the low-temperature air exiting
357   from the cavern, increasing the turbine power output.
358   The TES system is a key part of the storage process. For A-CAES plants the most suitable technology from both
359   technical and economic points of view is that based on the thermocline principle in a packed-bed of bulk solid material.
360   This storage technology operates a direct heat transfer between the air flowing inside the tank and a bulk solid material
361   filled in the tank. Reducing the air temperature inside the packed-bed from 600 to 35 °C allows the recovery of a mean
362   thermal power slightly lower than 40 MW. Globally, for 8 hours of charge phase the stored thermal energy can reach a
363   theoretical maximum value of about 315 MWh.
364   Due to its good specific heat capacity, wide availability and low cost, in this study gravel was chosen to fill the TES
365   system, although other materials such as beryllia (BeO) or zirconia (ZnO_2) require a smaller volume, due to the greater
366   volumetric heat capacity. Table 3 reports the main design parameters of the TES system:
367

Table 3. Main design parameters of the TES system

Theoretical maximum stored thermal energy	315 MWh
Filling material	Gravel
Average particle diameter	0.03 m
Void fraction	0.30
Material density	2750 kg/m^3
Material specific heat capacity	900 J/(kg·K)
Theoretical minimum bed volume	1930 m^3
Aspect ratio	2.5
Tank diameter	9.94 m
Tank height	24.85 m

368
369   A theoretical minimum bed volume of about 1930 m^3 was estimated, considering a void fraction ε equal to 0.30.
370
371
372   *3.4 Expansion system assumptions*
373
374   The compressed air stored in the cavern is released during the discharge phase and sent to the HP and LP turbines for
375   electricity production. At the beginning of the discharge phase, the air is released at about 100 bar and 35 °C. A pressure
376   drop in the pipes and TES in the range of 1–1.5 bar was estimated, mainly due to piping, whereas the pressure drop in the
377   TES system accounts just for several kPa. The high-pressure air out of the cavern is heated up in the TES system to a
378   maximum temperature of 600 °C. Due to the thermocline operating characteristics, as explained in the following, it is not
379   feasible to reach a TES outlet temperature of 600 °C for the whole duration of 3 hours of discharge. During this phase, the
380   cavern air pressure is reduced from 100 to 60 bar, while a constant outlet pressure of 30 bar was assumed (Table 4) for the
381   HPT. To allow the HPT to operate at a constant mass flow rate, pressure ratio and temperatures for a longer period, air
382   throttling upstream of the HPT can be carried out, imposing an HPT inlet pressure of about 70 bar for the first two hours,
383   when the TES system is able to heat the air to a constant temperature of 600 °C. Moreover, depending on the operating
384   conditions, an air mass flow partialisation can also be carried out downstream of the TES system, splitting the high-
385   temperature air flow through a 3-way throttle valve. The main air flow feeds the HPT, while a secondary flow bypasses
386   the HPT turbine and is mixed with the HPT exhaust, allowing an increase of the air temperature at the LPT inlet up to the
387   nominal operating value.
388   During the discharge phase the HPT pressure ratio can vary from a maximum of 3.30 to a minimum of 1.95. A single-
389   stage radial turbine was chosen as the HPT, due to its high expansion pressure ratio per stage, high reliability, low cost and

390 low longitudinal size. The variability of the expansion pressure ratio can be managed by changing the stagger angle of the
391 nozzles. An axial turbine was chosen for the LP section, since the expansion pressure ratio is considerably greater (slightly
392 lower than 30) than the HPT one. Axial turbines allow a better coupling of stages in comparison to radial ones, despite a
393 lower stage pressure ratio. Moreover, axial turbines are more suitable for large power output and volumetric flow rates. A
394 pressure loss of about 1% at the LP turbine exhaust was also considered. Table 4 reports the main design characteristics of
395 the two turbines:
396

Table 4. Main design parameters of the turbines

Turbine	HPT	LPT
Air mass flow	173.0 kg/s	173.0 kg/s
Turbine inlet pressure	72.0 – 99.0 bar [1]	30.0 bar
Turbine inlet temperature	600 °C	448 – 400 °C
Pressure ratio	2.40 – 3.30	29.4
Turbine outlet pressure	30.0 bar	1.02 bar
Polytropic efficiency	0.835	0.852

397
398
399 ## 4. System operation and performance

400 A detailed analysis of the operational phases of the A-CAES system and an in-depth evaluation of its performance in a
401 charge-discharge cycle were performed and are discussed in the following. First, the operation of the compression train
402 was simulated and the performance evaluated as a function of the cavern backpressure. The TES charge and discharge
403 processes were also analyzed and, in particular, both processes were optimized, maximizing the thermal energy released in
404 the discharge phase. Finally, two different operating modes for managing HP and LP turbines (with or without air
405 throttling) were analyzed and compared. The performance of the compression and expansion trains was predicted through
406 several simulation models developed using the GateCycle software platform, while a Matlab simulation model was
407 developed to predict the performance of the thermal energy storage system.
408
409 *4.1 Compression train operation*

410 As already mentioned, in the charge phase, both the axial compressors (LPC and IPC) operate in the design condition,
411 while the HP centrifugal compressor operates with a variable pressure ratio ranging from 1.62 to 2.71, depending on the
412 cavern backpressure. To operate as close as possible to design conditions, the axial compressors require to be fed by a
413 constant air mass flow. Consequently, the pressure ratio of the centrifugal compressor which follows can be adjusted, at
414 constant rotation speed, only by acting on the DGV. A detailed performance analysis was carried out referring to the
415 characteristic performance curves of an industrial reference compressor, expressed in terms of pressure ratio and
416 volumetric flow rate. Figure 2 shows the behaviour of the centrifugal compressor isentropic efficiency as a function of the
417 outlet pressure in the operating range 60–100 bar (pressure ratio in the range 1.62–2.71).
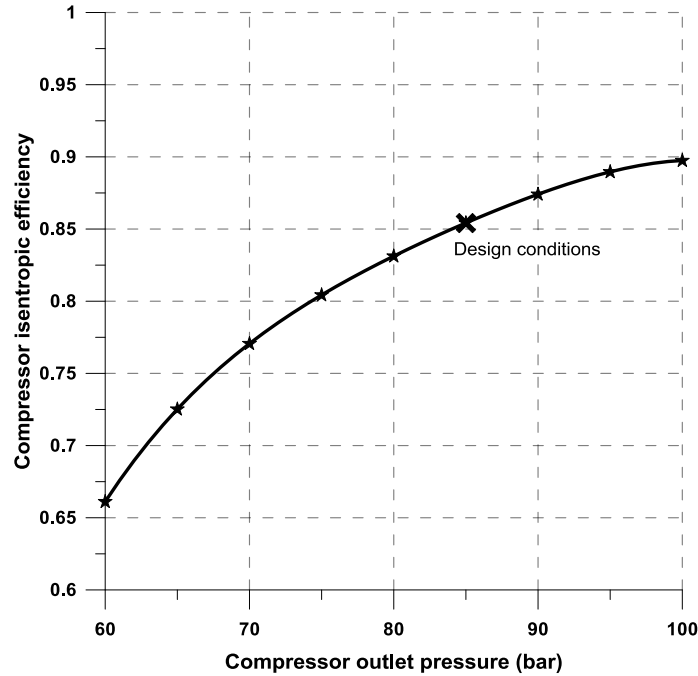418

[1] With or without air throttling

Figure 2. Isentropic efficiency of the centrifugal
compressor as a function of outlet pressure

419

420   The HPC design conditions were set at an output pressure of 85 bar (with a pressure ratio of 2.30), with a
421   corresponding isentropic efficiency equal to 0.854. Despite a remarkable efficiency reduction for lower values of the
422   outlet pressure, the influence on the total energy requirements is not substantial, since the power absorbed by the HPC is
423   significantly lower than the power absorbed by the LPC and IPC. Indeed, it is more important that both axial compressors
424   (LPC and IPC) operate as close as possible to nominal conditions in order to avoid an excessive increase of the power
425   absorbed and operational instability. Consequently, the LPC and IPC require a constant power of 24.5 and 16.9 MW
426   respectively, whereas the power required by the HPC ranges from about 4.5 MW to about 7.5 MW, being the pressure
427   ratio variation completely ascribed to the HPC. The total power required by the compressor train ranges from 45.9 MW
428   (cavern backpressure equal to 60 bar) to 48.8 MW (100 bar). Globally, during the 8-hour charge phase, the compression
429   train absorbs an electrical energy of about 380 MWh. Table 5 summarizes the main performance of the three compressors.
430   In particular, the performance of the HPC is reported with reference to operating pressures of 60, 85 and 100 bar.
431

Table 5. Compressor efficiency, pressure ratio β and power as a function of cavern pressure

Compressor	η_{IS}	β	$P\ [MW]$
LPC	0.888	13.0	24.47
IPC	0.885	2.81	16.87
HPC (60 bar)	0.661	1.62	4.61
HPC (85 bar, nominal conditions)	0.854	2.30	6.40
HPC (100 bar)	0.897	2.71	7.43

432

433   The HPC outlet temperature depends on the pressure ratio, ranging from 88 °C (β=1.62) to 118 °C (β=2.71). Due to
434   the relatively low temperature of the compressed air, a further thermal energy recovery was not performed downstream of
435   the HPC. Consequently, a water cooler was considered to dissipate thermal energy upstream of the storage cavern.

436

437   *4.2 Thermal energy storage system operation*

438

439　　　　The operation of the TES system was simulated through a two-equation, one-dimensional, transient model previously
440　developed at DIMCM [54], based on the work originally developed by Schumann [55]. Starting from the thermo-physical
441　properties of the filling solid material and of the heat transfer fluid and of the tank geometry, the model makes it possible
442　to predict, separately, the time evolution of the spatial distribution of both the fluid and solid temperature. The model is
443　based on the following assumptions and simplifications:

444　　　-　the temperature of both fluid and filling material is a function of time and the axial coordinate;
445　　　-　the fluid flow is considered incompressible (Mach number much lower than 0.3);
446　　　-　thermal properties of both gas and solid phase are temperature-dependent;
447　　　-　a uniform temperature distribution inside the solid (filling) material is considered;
448　　　-　the bed of solid material is isotropic and homogeneous and the heat transfer by conduction among solid particles
449　　　　is neglected;
450　　　-　heat transfer by natural convection and by radiation is neglected;
451　　　-　thermal conduction and external thermal losses are negligible.

452　　　　On the basis of these assumptions, the two-equation model for the fluid (3) and solid (4) phases along the axis of the
453　bed was established as follows:

454
455
456

$$\varepsilon\,(\rho C_v)_f\,\frac{\partial T_f}{\partial t} + \left(\rho C_p\right)_f u\frac{\partial T_f}{\partial x} = k_{eff}\,\frac{\partial^2 T_f}{\partial x^2} + h_{sf}\alpha_{sf}(T_s - T_f) \tag{3}$$

457

$$(1-\varepsilon)\,(\rho C)_s\,\frac{\partial T_s}{\partial t} = h_{sf}\alpha_{sf}(T_f - T_s) \tag{4}$$

458

459　where T and ρ are temperature and density, C_v and C_p the specific heat capacity at constant volume and pressure, ε the
460　void fraction, u the flow velocity, k_{eff} the effective fluid–solid conductivity, h_{sf}, the convective heat transfer coefficient,
461　α_{sf} the specific surface area, t the time, x the distance along the tank axial direction. The subscripts f and s refer to the
462　fluid and solid bed, respectively.
463　A detailed description of the model and of the expressions of the heat transfer coefficient h_{sf} and of the specific surface
464　area α_{sf} is reported in [54].
465　　　　In this study the aforementioned model was applied to evaluate the temperature distribution alongside the tank as a
466　function of both time and the number of cycles. In particular, assuming a null state of charge (SOC) of the tank as the
467　initial condition, for each charge-discharge cycle, the tank SOC was evaluated at the end of the charge or discharge phase.
468　Furthermore, a TES key parameter is the useful energy released during the discharge process. The analysis shows that the
469　tank should be oversized to avoid an excessive rise of the air outlet temperature during the charge phase. In fact, the TES
470　system allows only a partial discharge of the thermal energy accumulated and a large amount of thermal energy remains
471　inside the tank. Table 6 reports the main operating parameters of the TES system:
472

Table 6. Main TES operating parameters

Number of cycles	365
Tank diameter	10 m
Tank height	20/ 25/ 30 m
Aspect ratio	2/ 2.5/ 3
Tank volume	1570/ 1964/ 2355 m^3
Design TES outlet temperature in charge phase	35 °C

Design TES outlet temperature in discharge phase	600 °C

As reported in Table 6, the analysis of the TES system performance was carried out considering different values of the tank volume, placed in a vertical position. In particular, the tank diameter was fixed equal to 10 m, to maintain constant the thermo-fluid dynamics of the gas flow inside the tank, and different values of the tank height (20, 25, 30 m) were considered, corresponding to aspect ratio (AR) values equal to 2, 2.5 and 3, respectively. Up to 365 cycles were performed (assuming a charge-discharge cycle per day within a year) to evaluate the minimum number of cycles needed to reach a stable condition, for the 3 different values of AR. Once the TES system reaches a stable condition, the temperature distribution no longer changes significantly between one cycle and the next. During the charge phase the thermocline moves from top to bottom and the air temperature at the outlet of the TES system remains constant at the design condition (35 °C). When the thermocline approaches the bottom of the bed, the air outlet temperature starts to increase, with a different behaviour depending on the number of cycles and the aspect ratio. Similar behaviour takes place during the discharge phase, in which the air outlet temperature starts to decrease with respect to the design conditions (600 °C) when the thermocline approaches the top of the bed. Both these phenomena conventionally indicate the end of the charge and discharge phase respectively.

Figures 3a-3c show the temperature distribution alongside the tank axis for the three different values of tank height (20, 25, 30 m), to which correspond three different aspect ratios (2, 2.5, 3) at the end of the 8 hours of charge phase (red lines) and at the end of the 3 hours of discharge phase (blue lines), from the 1st to the 365th cycle. The area between the charge and discharge curve, for a given cycle, represents an index of the useful thermal energy released by the storage system. The zero value of the tank height in Figure 3 conventionally corresponds to the upper section of the TES system, where the warmest gas enters during the charge phase and exits during the discharge phase.
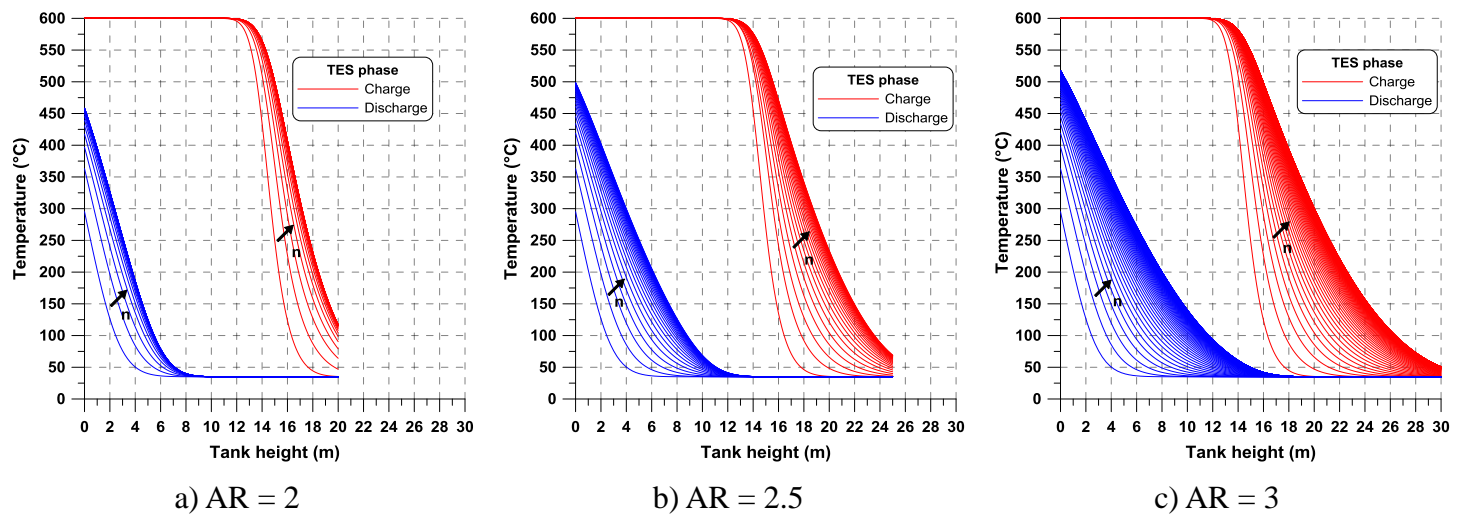

a) AR = 2 b) AR = 2.5 c) AR = 3

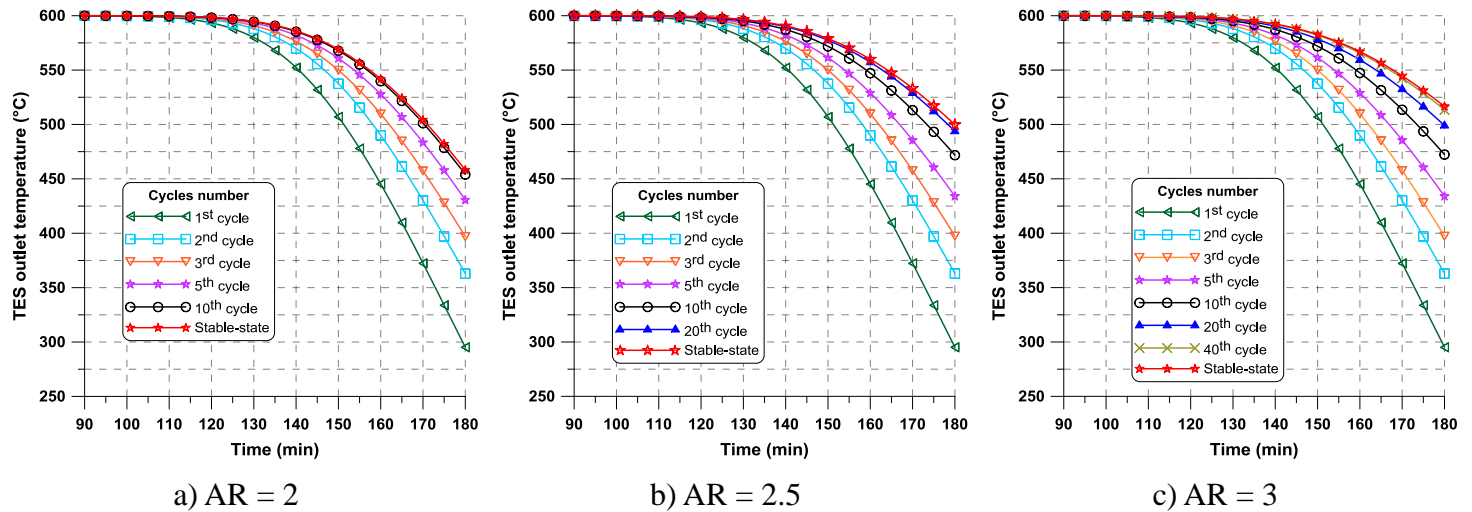**Figure 3.** Charge and discharge temperature inside the TES system as a function of number of cycles n and tank height

Figures 3a-3c show that the air outlet temperature increases after the first cycles in both the charge and discharge phase, finally reaching a steady-state value that is significantly dependent on the aspect ratio. At the end of charge, the air outlet temperature decreases, increasing the tank height, and the contrary occurs at the end of discharge, leading to a higher TIT and, consequently, to a greater energy production by the gas turbines. In particular, the air outlet temperature at the end of charging is equal to 35 °C (initial set value) in the first cycle, but it swiftly increases with the number of cycles. A higher temperature allows the charge level of the TES system to be increased, even if a greater amount of thermal energy must be dissipated by the intercooler to assure an almost constant temperature of the air at the HPC inlet. At stable conditions, the air outlet temperature is slightly lower than 120 °C for AR=2 and decreases to about 70 °C and 50 °C for AR= 2.5 and 3, respectively. At the end of discharge, at stable conditions, the best results are obtained with AR= 3, leading to an air outlet temperature of about 520 °C. Lower values, about 500 and 460 °C, are reached with AR=2.5 and 2 respectively. Figures 3a-3c also show that the TES system converges to stable conditions after a given number of cycles

506 dependent on the aspect ratio (that is, on the tank height). A lower value of AR allows a faster convergence to be achieved
507 and thus to a stable condition being quickly reached after a plant shutdown. On the other hand, it also leads to a lower
508 TES outlet temperature at the end of the discharge phase due to the lower storage capacity.
509   Figures 4a-4c show the air temperature at the outlet of the TES system in the discharge phase as a function of time and
510 the number of cycles, for AR=2, 2.5 and 3, respectively. Firstly, it can be seen that stable conditions are practically
511 reached after about 10, 20 and 40 cycles for AR equal to 2, 2.5 and 3 respectively. Moving from the first cycle towards
512 stability, as already seen in Figures 3a-3c, the air outlet temperature strongly increases.
513

a) AR = 2   b) AR = 2.5   c) AR = 3

Figures 4. TES outlet temperature in the discharge phase as a function of time and number of cycles

514
515   Moreover, when increasing the number of cycles, the air exiting the TES lasts longer at a constant temperature of 600
516 °C, but this feature is poorly influenced by the aspect ratio. In fact, at stable conditions, the air outlet temperature lasts at
517 600 °C for 111, 114 and 116 minutes, for AR equal to 2.5, 3 and 3.5 respectively. As previously mentioned, the air outlet
518 temperature during discharge is a key parameter. In fact, reducing this temperature not only causes a lower HPT power
519 output, but can also lead to a LPT outlet temperature below 25 °C.
520   Finally, a preliminary analysis was carried out to evaluate the influence of the aspect ratio and of the number of cycles
521 on both the air temperature at the LPT outlet and the overall gas turbine energy production. In this analysis, an isentropic
522 efficiency of both HPT and LPT equal to 0.90 was assumed and pressure losses were neglected.
523   At the beginning of discharge phase (HPT inlet conditions equal to 600 °C and 100 bar), the LPT outlet temperature is
524 about 40 °C. For the next 2 hours, the TES outlet temperature is constantly equal to 600 °C and the LPT outlet
525 temperature increases, due to the reduction of the HPT inlet pressure. When the TES outlet temperature starts to decrease
526 (last hour), the LPT outlet temperature decreases greatly and drops below 25 °C. Moreover, as the TES outlet temperature
527 increases with the number of cycles, the LPT outlet temperature also increases up to stable conditions. Nevertheless, for
528 AR=2 the LPT exhaust temperature drops below 25 °C, also at TES stable conditions, whereas for AR=2.5 and AR=3,
529 stable conditions lead to exhaust temperatures equal to about 30 and 40 °C respectively. However, during the first cycles,
530 a pressure reduction, by throttling upstream of the LPT, is required also for AR=2.5 and AR=3 to avoid an exhaust
531 temperature below 25 °C.
532   Figure 5 shows the energy produced by the A-CAES plant during the discharge process as a function of the number of
533 cycles for the three values of AR considered in this paper. In particular, the figure shows that despite a 100 MW-size
534 turbine operating for 3 hours, the energy production is lower than 300 MWh. In fact, the A-CAES power output decreases
535 during the discharge phase, due to the reduction of both pressure and temperature at the HPT inlet.
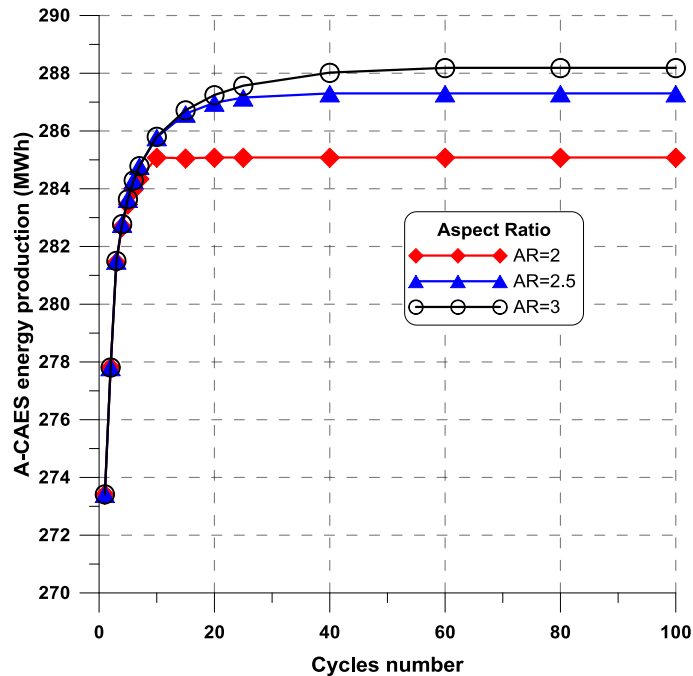536

Figure 5. Energy produced by turbine as a function of AR
and number of cycles

The energy production increases with the number of cycles until reaching stable conditions. Conversely, the tank aspect ratio does not significantly influence the energy production. As the power output depends strictly on the air temperature at the outlet of the TES system (Figures 4a-4c), the first cycles show the same trend for each AR. By contrast, when increasing the number of cycles, a greater AR leads to a slightly greater energy production due to the higher volume of the storage system. In particular, at the end of the discharge phase, the power output at stable conditions increases from 78 to 85 MW, varying AR from 2 to 3. Globally, at stable conditions the energy production is equal to about 288 MWh for AR=3, 287 MWh for AR=2.5 and 285 MWh for AR=2. Furthermore, already from the 10th cycle, both AR=2.5 and AR=3 assure a higher energy production than AR=2 at stable conditions.

Finally, considering that the energy production for AR=2.5 is only 0.35% less than for AR=3 and that for AR=2 the LPT exhaust temperature drops below 25 °C, a tank height of 25 m, corresponding to an aspect ratio of 2.5, was chosen as a reference case for the evaluation of the expansion train performance.

In fact, despite a slightly lower energy production, a lower AR, and consequently a smaller volume of the TES system, allows a reduction of costs, in terms of both capital and filling materials. On the other hand, the higher air outlet temperature in the charge phase requires a slightly larger intercooler to cool the air at the HPC inlet.

4.3 Expansion train operation

Two different operating modes for the discharge process were evaluated, with and without throttling the compressed air at the HP turbine inlet.

    a.   Case with air throttling upstream of the HP turbine

During the first two hours of the discharge phase, when the TES outlet temperature remains around 600 °C, the compressed air upstream of the HPT is throttled to about 72 bar, assumed as the nominal inlet pressure, leading the turbine to operate at nominal conditions for about 2/3 (2 hours) of the whole discharge phase. Moreover, the air throttling avoids an excessive deviation from the design conditions during the 3rd hour, when the HPT operates at variable conditions (flow rate, inlet pressure and temperature). This operating mode allows the LPT to operate at nominal conditions during the

564 entire discharge phase, assuring a constant LPT inlet pressure (around 30 bar) by acting on the nozzle stagger angle of the
565 HPT to control the expansion ratio. In particular operating conditions, a fraction of the compressed air flow exiting the
566 TES system bypasses the HPT and mixes with the air entering the LPT for heating it up to the design temperature (slightly
567 lower than 450 °C). Figure 6 shows the behaviour of the HPT inlet pressure and temperature as a function of time, in the
568 case of air throttling, together with the TES outlet pressure at stable conditions.
569
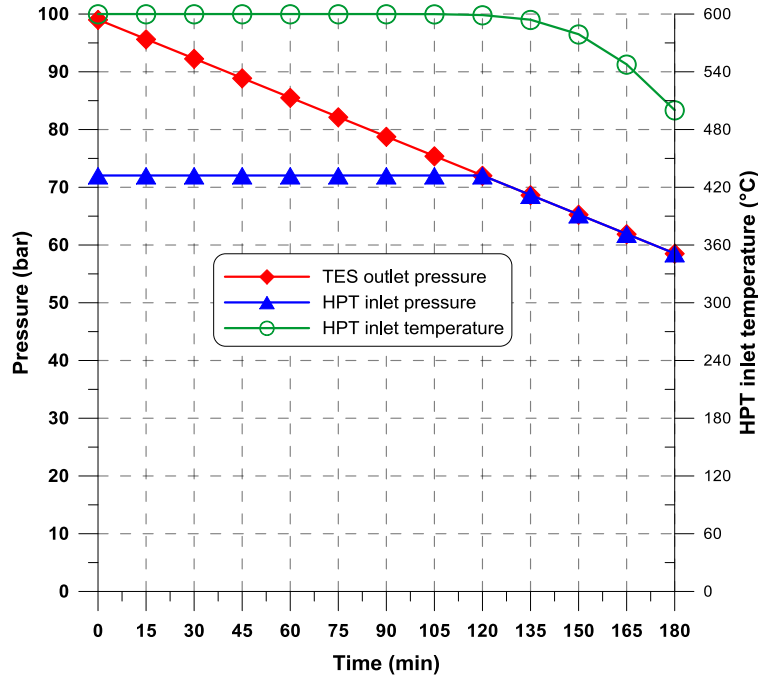
Figure 6. TES outlet pressure and HPT inlet pressure and temperature as a function of time. Throttling case (AR=2.5)

570
571   As the HPT expansion ratio deviates slightly from nominal conditions (from 2.40 to 1.95, after 180 minutes) during
572 the last third of the discharge, a constant HPT isentropic efficiency (in this case equal to 0.85) was assumed. A constant
573 isentropic efficiency of 0.90 was also assumed for the LPT, since it operates at design conditions for the whole discharge
574 phase. Table 7 summarizes the main HPT and LPT characteristics at nominal conditions for the case with air throttling.
575

Table 7. Main HPT and LPT characteristics at design conditions

Turbine	HPT	LPT
Air mass flow	173.0 kg/s	173.0 kg/s
Turbine inlet pressure	72 bar	30 bar
Turbine inlet temperature	600 °C	448 °C
Pressure ratio	2.40	29.6
Turbine outlet pressure	30 bar	1.02 bar
Turbine outlet temperature	448 °C	54 °C
Isentropic efficiency	0.85	0.9

576
577
578   b.   Case without air throttling upstream of the HP turbine

579   In this operating mode, the compressed air from the TES system is not throttled upstream of the HPT and the HPT
580 inlet pressure varies during the entire discharge phase between 99.0 and 58.5 bar (Figure 6, TES outlet pressure).

581 Consequently, both gas turbines operate at off-design conditions during all 3 hours of discharge. Also in this case, the LPT
582 inlet pressure is maintained almost constant (around 30 bar) by acting on the nozzle stagger angle to control the HPT
583 expansion ratio. In this case, air splitting upstream of the HPT is performed just to prevent an LPT discharge temperature
584 below the set value of 25 °C. The design isentropic efficiency was set still equal to 0.85 and 0.90 for the HPT and LPT,
585 respectively.
586
587
588 *4.3.1 Results for case with air throttling upstream of the HP turbine*
589   The air mass flow bypassing the HPT was evaluated, for different TES cycles, by imposing an air temperature at the
590 LPT inlet equal to the nominal value (448 °C) and, in extreme conditions, the minimum allowed LPT outlet temperature
591 (25 °C). Finally, the power output and energy produced by both the HP and LP turbines were evaluated as a function of
592 time for each TES cycle.
593   The HPT air outlet temperature is influenced by both the HPT pressure ratio and the inlet temperature (corresponding
594 to the temperature at the outlet of the TES system). As shown by Figure 6, the HPT inlet pressure is set equal to 72.0 bar
595 for about 120 minutes. In the remaining 60 minutes, it decreases to 58.5 bar and is not influenced by the number of TES
596 cycles. On the contrary, as shown by Figure 4b, the TES outlet temperature decreases with time and increases with the
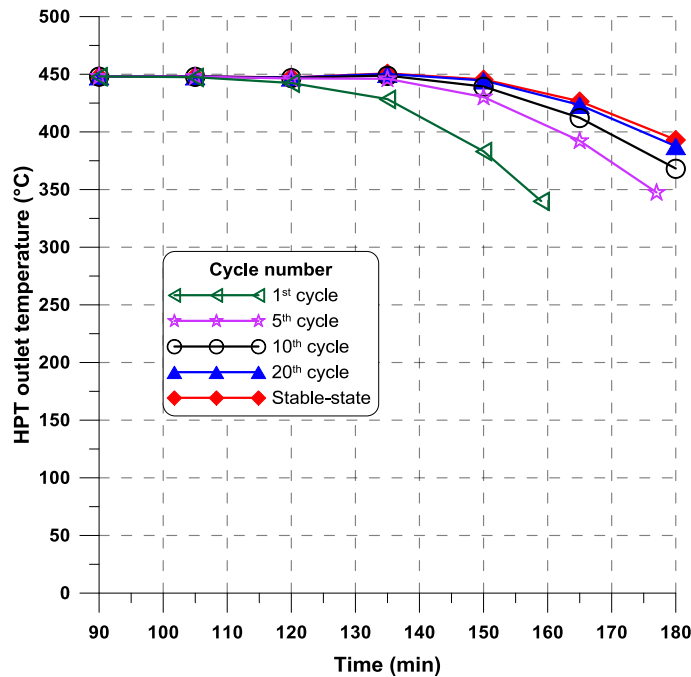597 number of cycles. Figure 7 shows the HPT outlet temperature as a function of time and for several TES cycles.
598

Figure 7. HPT outlet temperature as a function of time
and number of cycles (AR=2.5)

599
600   During the first two hours, the air throttling allows operation at design conditions, leading to a constant HPT outlet
601 temperature (slightly lower than 450 °C). During the 3rd hour, despite a lower pressure ratio, the substantial reduction of
602 the HPT inlet temperature strongly affects the HPT outlet temperature. Figure 7 shows that the HPT outlet temperature
603 drops far below the nominal value and the exhaust air needs to be heated by the high-temperature air bypassing the HPT,
604 in order to keep the nominal temperature value (448 °C) at the LPT inlet. At stable conditions, for example, the HPT
605 exhaust temperature decreases to about 390 °C, while lower HPT outlet temperatures, even below 350 °C, are reached
606 during the first cycles. The HPT outlet temperature is not reported in Figure 7 for the last three minutes of the 5th cycle
607 and for the last twenty of the 1st cycle, since the air temperature at the outlet of the TES system drops below 448 °C
608 (Figure 4b). In this case, the HPT is fully bypassed and the air is throttled up to 30 bar in order to ensure that the LPT

609 operates close to the design conditions. Figure 8 shows the fraction of air bypassing the HPT as a function of time and the
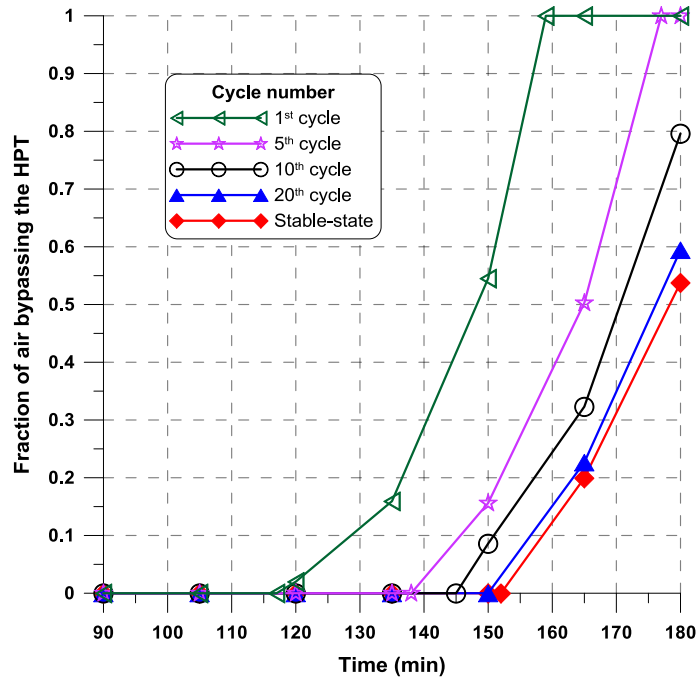610 number of cycles.
611

Figure 8. Fraction of air bypassing the HPT as a function
of time and number of cycles (AR=2.5)

612
613   As shown by Figure 8, the bypass is not required in the first two hours and it starts when the HPT outlet temperature
614 starts to decrease below 448 °C. At stable cycle conditions (practically after the 20th cycle), the fraction of air split reaches
615 a maximum value around 55–60% at the end of the discharge phase. In the early cycles, the fraction of air to be split is
616 larger. As previously mentioned, the HPT is fully bypassed in the last 3 minutes of the 5th cycle and in the last 20 of the 1st
617 cycle. In the first cycles, moreover, a further air throttle (up to a minimum value of 14.5 bar) could be required upstream
618 of the LPT to avoid an exhaust temperature lower than 25 °C.
619   At the HPT inlet the deviation of volumetric flow from the design values is quite moderate (lower than 10%) during
620 almost all the discharge phase. For this reason, the HPT efficiency was assumed to remain constant, also considering that
621 the power output of the HPT turbine is only about 30% of the total power output. Conversely, the LPT is characterized by
622 a virtually constant volumetric flow rate throughout the discharge phase, since the inlet conditions are close to the design
623 values. Figure 9 reports the power output of the HPT and the overall power output of the A-CAES plant as a function of
624 time and the number of cycles. The power output of the LPT is not reported in Figure 9 since it operates for the entire
625 discharge interval with a constant power output (70.8 MW), except for the last 15 minutes of the first cycle and the last
626 three of the 5th cycle. During this period, the HPT is bypassed and an air throttling is carried out before the LPT, so that
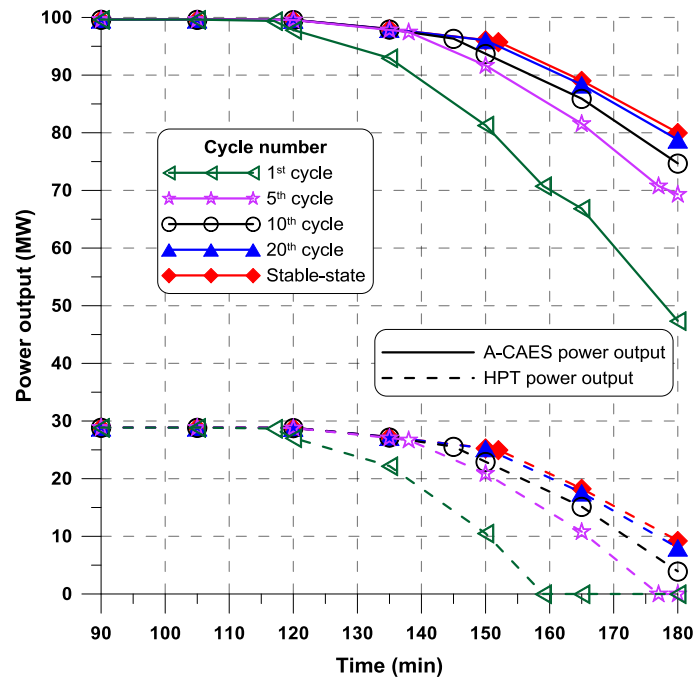627 the power output of the A-CAES plant drops below 70 MW.
628

Figure 9. A-CAES power and HPT power as a function of
time and number of cycles (AR=2.5)

The power output of the HPT (and consequently of the A-CAES plant) is constant for about the first 2 hours and decreases in the last hour (a little more for the first 5 cycles). The overall A-CAES design power output is equal to 97.6 MW, while the HPT power output is equal to 28.3 MW. Minimum values of the HPT power output, and consequently of the A-CAES plant, are reached at the end of the discharge phase and increase with the number of cycles. At stable conditions, the overall A-CAES power output is a little lower than 80 MW, due to a very low HPT power output, equal to 9.0 MW, whereas a stronger depowering is present in the first 5 cycles. During the last 3 minutes of the 5th and 20 minutes of the 1st cycle, in particular, the HPT power output is null (HPT fully bypassed) and a minimum value of the A-CAES power output equal to 46.4 MW is reached at the end of the 1st cycle, when also the LPT operates far from the design conditions.

4.3.2 Results for case without air throttling upstream of the HP turbine

With this operating mode, the air mass flow bypassing the HPT was evaluated, for different charge/discharge cycles, just imposing a LPT minimum outlet temperature (25 °C). The absence of the air bypass upstream of the HPT for a large time interval leads to a variable air temperature at the LPT inlet. The power output and energy produced by both the HPT and LPT were also evaluated as a function of time for each operating cycle. Figure 10 shows the temperature of the air at the HPT outlet as a function of time and the number of cycles.
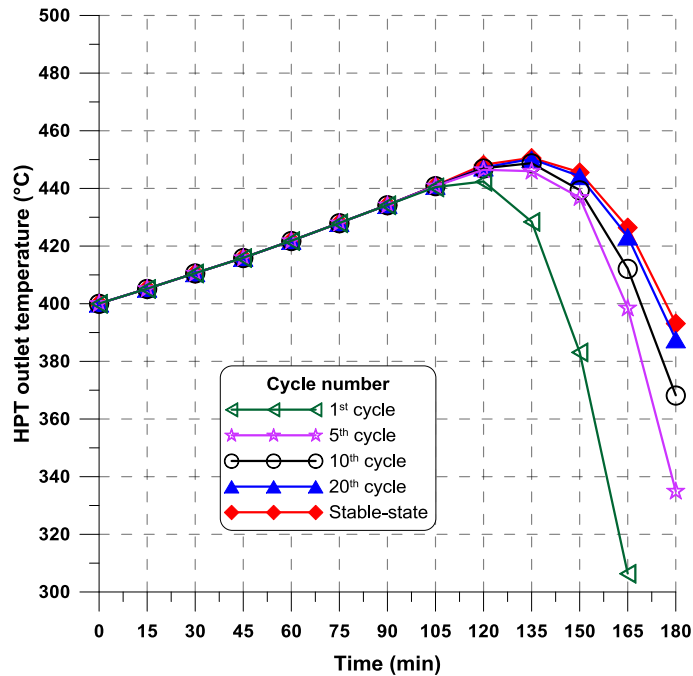
Figure 10. HPT outlet temperature as a function of time
and number of cycles (AR=2.5)

At the beginning of the discharge phase, the HPT outlet temperature is equal to 400 °C. For the first two hours, the TES system allows the air to be heated up to around 600 °C (Figure 4b) and the decrease of the HPT inlet pressure (corresponding to the TES outlet pressure reported in Figure 6) leads to an increase of the HPT outlet temperature up to a value slightly lower than 450 °C (nominal condition for throttling case). In the last hour, the decrease of the HPT inlet temperature overcomes the reduction of the pressure ratio, leading to a strong reduction of the HPT outlet temperature (more marked in the first cycles). As mentioned, the air bypass is only required, in some particular conditions, for avoiding a LPT outlet temperature lower than 25 °C. In this way, both the HPT and LPT operate at off-design conditions for a large time interval. The design conditions were chosen, for both the turbines, in order to minimize volume flow variations. In particular, for the HPT the design conditions occur after 1 hour and 45 minutes, while for the LPT after 1 hour. The volumetric flow rate of the air entering the HPT ranges from -22.3% to + 16.4% with respect to the design conditions. Despite such a variation, a constant isentropic efficiency (85%) was considered. For the LPT the variation of the volumetric flow rate is considerably lower, from -3.5% to 4.0%, and also in this case the efficiency was assumed constant and equal to 90%. Figure 11 shows the fraction of air bypassing the HPT as a function of time and the number of cycles.
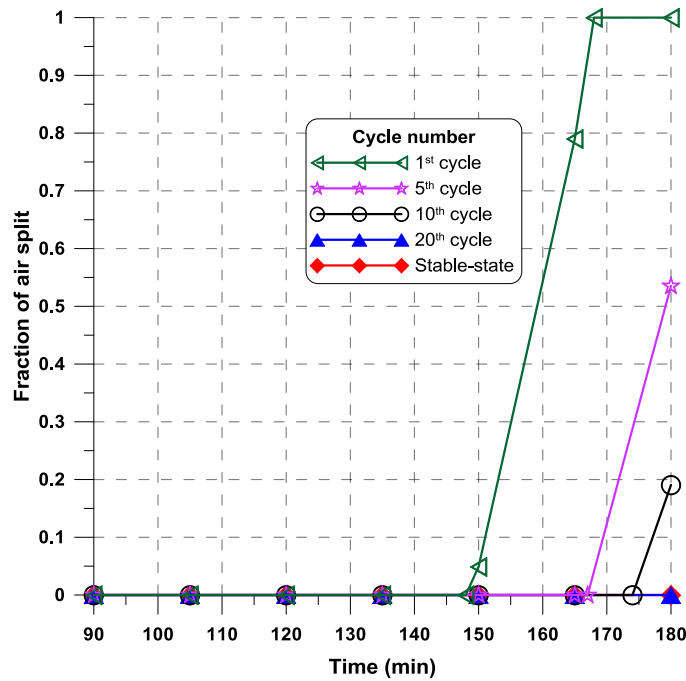
Figure 11. Fraction of air bypassing the HPT as a
function of time and number of cycles (AR=2.5)

663
664   Figure 11 shows that the air bypass is not required after the 20th cycle (when stable conditions are almost reached),
665   since the LPT exhaust temperature exceeds 25 °C during the entire discharge phase. In the 10th and 5th cycles the air
666   splitting is required just in the last 5–15 minutes and the fraction of air split reaches a maximum value of 19% and 54%
667   respectively. In the 1st cycle, the air splitting upstream of the HPT is required starting about half an hour before the end of
668   the discharge phase. In the last 12 minutes both a bypass of the HPT and a pressure throttle upstream of the LPT (up to a
669   minimum value of 14.5 bar) are performed in order to reach an exhaust temperature higher than 25 °C.
670   Figure 12 reports the power output of the HPT and LPT and the overall power output of the A-CAES plant as a
671   function of time and the number of cycles. Both the HPT and LPT show a variable power output since they operate at off-
672   design conditions during the whole discharge phase. The HPT power output decreases with time due to the simultaneous
673   reduction of the inlet temperature and pressure ratio. On the contrary, the LPT power output only depends on the air inlet
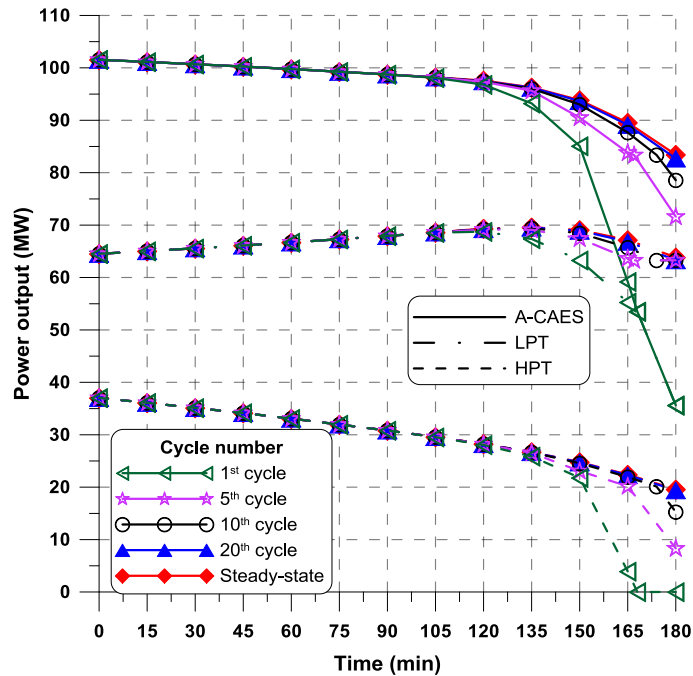674   temperature, the expansion pressure ratio being constant.
675

Figure 12. A-CAES, LPT and HPT power as a function of
time and number of cycles (AR=2.5)

At stable conditions (practically after the 20th cycle), the overall power output varies from a maximum of about 102 MW to a minimum of about 83 MW. The HPT power output decreases from 37 to 19 MW, whereas the LPT ranges between 64 and 70 MW. In the early cycles, a strong power output reduction occurs in the third hour of the discharge phase, due to the operation of the air bypass that causes a reduction of the HPT power output compared to stable conditions. At the end of the 1st cycle, the overall power output drops to about 35 MW, due to both the bypass of the HP turbine and the air throttling upstream of the LPT with a pressure reduction up to 14.5 bar.

4.3.3 Comparison of the two configurations

Table 8 reports the overall energy production and the round trip efficiency, calculated by Eq. (2), for the two operation modes previously described and for several reference number of cycles.

Table 8. Global energy production and round trip efficiency

Number of cycles	Energy production (MWh)		Round trip efficiency (%)	
	Throttling case	No throttling case	Throttling case	No throttling case
1	270.9	276.5	71.5	73.0
5	282.2	288.0	74.5	76.0
10	284.5	289.6	75.0	76.4
20	286.1	291.6	75.5	76.9
Stable-state	286.5	291.9	75.6	77.0

As expected, at stable conditions the air throttling reduces the overall energy production, from 292 to 286.5 MWh. In both operating modes the energy production is noticeably lower in the early cycles, becoming almost steady after the 20th cycle as previously highlighted. Moreover, the energy difference between the two operating modes, about 5–6 MWh, is

692 almost independent of the number of cycles. Indeed, the difference in energy production should be even smaller
693 considering the real behaviour of the turbines efficiency in off-design operating conditions.
694   In the absence of air throttling upstream of the HPT, both the HPT and LPT operate at off-design conditions for the
695 whole duration of the discharge phase. Conversely, the air throttling upstream of the HPT allows the LPT to operate
696 constantly at the design condition and the HPT for about 2 hours, while in the last hour it operates not so far from the
697 design point. Furthermore, since about 70% of the overall energy production is ascribed to the LP turbine, it may be
698 appropriate for the LPT to operate as close as possible to the design conditions. Therefore, the choice between the two
699 solutions should be guided by a proper assessment of the control and management of the machinery and of the entire
700 system in off-design operating conditions.
701   The round trip efficiency is given by the ratio between the electrical energy E_T produced by the turbine train and the
702 electrical energy E_M required by the compressor train, the fuel chemical energy E_F being null. The total energy required
703 by the compressor E_M during the charge phase is equal to 379.0 MWh, leading to values of the round trip efficiency
704 ranging from 71.5% (first cycle of throttling case) to 77.0% (stable conditions of no throttling case), depending strictly on
705 the energy production. The difference between the two operating modes is about 1.5% at stable conditions. Such values
706 are considerably higher than those of D-CAES plants [9,10] and slightly higher, but comparable with those expected by
707 R&D studies on A-CAES, where efficiencies exceeding 70% are reported [16,56].

708
709
710   **CONCLUSIONS**

711   This paper reports an in-depth study of an adiabatic CAES (A-CAES) plant integrated with a packed-bed thermocline
712 thermal energy storage system, proposing a novel A-CAES configuration and operation mode. Several simulation models
713 were developed to evaluate the performance of the A-CAES plant and TES system, in both design and off-design
714 operation. The A-CAES plant studied is characterized by a nominal power output equal to about 100 MW and a charge-
715 discharge cycle per day, with an 8-hour charge and 3-hour discharge for continuous electrical generation.
716   The operation of the compression train, based on two axial compressors (LPC and IPC) and a centrifugal compressor
717 (HPC), was simulated predicting the performance as a function of the cavern backpressure. The total power required by
718 the compressor train ranges from 45 to 50 MW, varying the cavern backpressure from 60 to 100 bar. Globally, during the
719 8-hour charge phase, the compression train absorbs an electrical energy of about 380 MWh. The configuration of the
720 compressor train was chosen in order to fully ascribe the pressure ratio variation to the HP centrifugal compressor, since
721 its influence on the total energy requirements is not relevant. Accordingly, both the LP and IP axial compressors operate
722 very close to nominal conditions, so as to avoid instability of operation and excessive increase of power absorption. In
723 fact, the power required by the HPC (ranging from about 4.5 MW to about 7.5 MW) is significantly lower than the power
724 absorbed by the LPC (24.5 MW) and IPC (16.9 MW).
725   The TES charge and discharge processes were also analyzed, integrated with the A-CAES plant and, in particular, both
726 processes were optimized, maximizing the suitable thermal energy in the discharge phase. The TES performance was
727 evaluated as a function of the number of cycles. For an aspect ratio equal to 2.5, the minimum number of cycles needed to
728 reach a stable condition (no significant changes of the temperature distribution between one cycle and the next) was in
729 practice about 20. Due to the thermocline operating characteristics, it is not feasible to maintain a TES outlet temperature
730 equal to the reference TIT, set at 600 °C, for the whole duration of the 3-hour discharge. In fact, the air outlet temperature
731 remains constant and equal to 600 °C for about 2 hours, and when the thermocline approaches the top of the bed it
732 noticeably decreases (especially for the first cycles). The discharge temperature of the TES system is a key parameter and
733 its decrease in fact not only leads to a lower HPT power output, but can also drop the LPT outlet temperature below the
734 minimum allowed temperature set at 25 °C.
735   Finally, two different operating modes for managing the turbines during the discharge process were analyzed. A first
736 mode assumes a throttling of the compressed air upstream of the HP turbine during the first two hours of the discharge
737 phase (TES outlet temperature around 600 °C). The air throttling leads the turbine to operate at nominal conditions for
738 about 2/3 of the whole discharge phase and avoids an excessive deviation from the design conditions during the 3rd hour,
739 when the HPT operates at variable conditions. When the TES outlet temperature starts to decrease, a fraction of the
740 compressed air flow bypasses the HPT and mixes with the air entering the LPT which is heated up to the design
741 temperature, allowing the LPT to operate at nominal conditions during the entire discharge phase. In the second operating

mode the compressed air is not throttled upstream of the HPT and the HPT inlet pressure varies during the entire discharge phase between about 99.0 and 58.5 bar. Consequently, both HP and LP turbines operate at off-design conditions during all 3 hours of discharge. In this case, the air splitting upstream of the HPT is performed just to prevent a LPT discharge temperature below the minimum allowed value of 25 °C. At nominal conditions, the A-CAES power output is about 100 MW, dropping to less than 40 MW in the last minutes of the first cycles. The overall energy production ranges between 271 and 292 MWh, depending on the number of cycles and the operating mode. The results show that operating without throttling allows an energy production that is theoretically greater by about 5–6 MWh, but requires operation at the off-design condition during the entire discharge process. As a consequence the performance of the configuration without throttling is affected by some uncertainty, due to the assumption of a constant isentropic efficiency for the turbines.

Globally, the A-CAES plant shows a round trip efficiency in the order of 0.71–0.77, depending strictly on the number of cycles and the turbine operation mode. Such values are considerably higher than those of D-CAES plants and are comparable with those expected by R&D studies on A-CAES.

REFERENCES

[1]   International Energy Agency. World Outlook Energy 2015. 2015. doi:10.1787/weo-2014-en.

[2]   Kyriakopoulos GL, Arabatzis G. Electrical energy storage systems in electricity generation: Energy policies, innovative technologies, and regulatory regimes. Renew Sustain Energy Rev 2016;56:1044–67. doi:10.1016/j.rser.2015.12.046.

[3]   Lamadrid AJ. Optimal use of energy storage systems with renewable energy sources. Int J Electr Power Energy Syst 2015;71:101–11. doi:10.1016/j.ijepes.2015.01.025.

[4]   Gallo AB, Simoes-Moreira JR, Costa HKM, Santos MM, Moutinho dos Santos E. Energy storage in the energy transition context: A technology review. Renew Sustain Energy Rev 2016;65:800–22. doi:10.1016/j.rser.2016.07.028.

[5]   Kaldellis JK. Chapter 13 - Photovoltaic-Energy Storage Systems for Remote Small Islands. 2015. doi:10.1016/B978-0-12-409540-3.00013-X.

[6]   López González E, Isorna Llerena F, Silva Pérez M, Rosa Iglesias F, Guerra Macho J, Isorna F, et al. Energy evaluation of a solar hydrogen storage facility: Comparison with other electrical energy storage technologies. Int J Hydrogen Energy 2015;40:5518–25. doi:10.1016/j.ijhydene.2015.01.181.

[7]   Barbour E, Wilson IAG, Radcliffe J, Ding Y, Li Y. A review of pumped hydro energy storage development in significant international electricity markets. Renew Sustain Energy Rev 2016;61:421–32. doi:10.1016/j.rser.2016.04.019.

[8]   Budt M, Wolf D, Span R, Yan J. A review on compressed air energy storage: Basic principles, past milestones and recent developments. Appl Energy 2016;170:250–68. doi:10.1016/j.apenergy.2016.02.108.

[9]   Crotogino F, Mohmeyer K-U, Scharf R. Huntorf CAES: More than 20 Years of Successful Operation. Solut Min Res Inst Spring Meet 2001:351–7.

[10]   De Biasi V. 110 MW McIntosh CAES plant over 90% availability and 95% reliability. Gas Turbine World 1998;28:26–8.

[11]   Liu J-L, Wang J-H. A comparative research of two adiabatic compressed air energy storage systems. Energy Convers Manag 2016;108:566–78. doi:10.1016/j.enconman.2015.11.049.

[12]   Yang K, Zhang Y, Li X, Xu J. Theoretical evaluation on the impact of heat exchanger in Advanced Adiabatic Compressed Air Energy Storage system. Energy Convers Manag 2014;86:1031–44. doi:10.1016/j.enconman.2014.06.062.

[13]   Bagdanavicius A, Jenkins N. Exergy and exergoeconomic analysis of a Compressed Air Energy Storage combined with a district energy system. Energy Convers Manag 2014;77:432–40. doi:10.1016/j.enconman.2013.09.063.

[14]   Zhao P, Dai Y, Wang J. Design and thermodynamic analysis of a hybrid energy storage system based on A-CAES (adiabatic compressed air energy storage) and FESS (flywheel energy storage system) for wind power application. Energy 2014;70:674–84. doi:10.1016/j.energy.2014.04.055.

[15]   Castellani B, Presciutti A, Filipponi M, Nicolini A, Rossi F. Experimental Investigation on the Effect of Phase Change Materials on Compressed Air Expansion in CAES Plants. Sustainability 2015;7:9773–86. doi:10.3390/su7089773.

[16]   Barbour E, Mignard D, Ding Y, Li Y. Adiabatic Compressed Air Energy Storage with packed bed thermal energy storage. Appl Energy 2015;155:804–15. doi:10.1016/j.apenergy.2015.06.019.

[17]   Lund H, Salgi G. The role of compressed air energy storage (CAES) in future sustainable energy systems. Energy Convers Manag 2009;50:1172–9. doi:10.1016/j.enconman.2009.01.032.

[18]   Lund H, Salgi G, Elmegaard B, Andersen AN. Optimal operation strategies of compressed air energy storage (CAES) on

795 electricity spot markets with fluctuating prices. Appl Therm Eng 2009;29:799–806.
796 doi:10.1016/j.applthermaleng.2008.05.020.

797 [19] Arabkoohsar A, Machado L, Farzaneh-Gord M, Koury RNN. Thermo-economic analysis and sizing of a PV plant equipped
798 with a compressed air energy storage system. Renew Energy 2015;83:491–509. doi:10.1016/j.renene.2015.05.005.

799 [20] Arabkoohsar A, Machado L, Koury RNN. Operation analysis of a photovoltaic plant integrated with a compressed air energy
800 storage system and a city gate station. Energy 2016;98:78–91. doi:10.1016/j.energy.2016.01.023.

801 [21] Zafirakis D, Kavadias K, Kondili EM, Kaldellis JK. Optimum sizing of PV-CAES configurations for the electrification of
802 remote consumers. Comput Aided Chem Eng 2014;33:1135–40. doi:10.1016/B978-0-444-63455-9.50024-6.

803 [22] Zunft S, Jakiel C, Koller M, Bullough C. Adiabatic Compressed Air Energy Storage for the Grid Integration of Wind Power.
804 Sixth Int. Work. Large-Scale Integr. Wind Power tTransmission Networks Offshore Wind., 2006, p. 26–8.

805 [23] Zhao P, Wang M, Wang J, Dai Y. A preliminary dynamic behaviors analysis of a hybrid energy storage system based on
806 adiabatic compressed air energy storage and flywheel energy storage system for wind power application. Energy
807 2015;84:825–39. doi:10.1016/j.energy.2015.03.067.

808 [24] Grazzini G, Milazzo A. Thermodynamic analysis of CAES/TES systems for renewable energy plants. Renew Energy
809 2008;33:1998–2006. doi:10.1016/j.renene.2007.12.003.

810 [25] Hartmann N, Vöhringer O, Kruck C, Eltrop L. Simulation and analysis of different adiabatic Compressed Air Energy Storage
811 plant configurations. Appl Energy 2012;93:541–8. doi:10.1016/j.apenergy.2011.12.007.

812 [26] Wolf D, Budt M. LTA-CAES - A low-temperature approach to adiabatic compressed air energy storage. Appl Energy
813 2014;125:158–64. doi:10.1016/j.apenergy.2014.03.013.

814 [27] Minutillo M, Lubrano Lavadera A, Jannelli E. Assessment of design and operating parameters for a small compressed air
815 energy storage system integrated with a stand-alone renewable power plant. J Energy Storage 2015;4:135–44.
816 doi:10.1016/j.est.2015.10.002.

817 [28] Manfrida G, Secchi R. Performance prediction of a Small-Size Adiabatic Compressed-Air Energy Storage system. Int J
818 Thermodyn 2015;18:111–9. doi:10.5541/ijot.71710.

819 [29] Garrison JB, Webber ME. An integrated energy storage scheme for a dispatchable solar and wind powered energy system. J
820 Renew Sustain Energy 2011;3. doi:10.1063/1.3599839.

821 [30] Rwe Power. Adele–Adiabatic Compressed-Air Energy Storage for Electricity Supply. Rep RWE Power n.d.:1–12.
822 https://www.rwe.com/web/cms/mediablob/en/391748/data/364260/1/rwe-power-ag/innovations/Brochure-ADELE.pdf.

823 [31] Patel S. First Megawatt-Scale Isothermal CAES Completion. Power 2013. http://www.powermag.com/first-megawatt-scale-
824 isothermal-caes-completion/.

825 [32] Van de Ven JD, Li PY. Liquid piston gas compression. Appl Energy 2009;86:2183–91. doi:10.1016/j.apenergy.2008.12.001.

826 [33] Qin C, Loth E. Liquid piston compression efficiency with droplet heat transfer. Appl Energy 2014;114:539–50.
827 doi:10.1016/j.apenergy.2013.10.005.

828 [34] Salvini C. Techno-Economic Analysis of CAES Systems Integrated into Gas-Steam Combined Plants. Energy Procedia
829 2016;101:870–7. doi:10.1016/j.egypro.2016.11.110.

830 [35] Zhao P, Dai Y, Wang J. Performance assessment and optimization of a combined heat and power system based on compressed
831 air energy storage system and humid air turbine cycle. Energy Convers Manag 2015;103:562–72.
832 doi:10.1016/j.enconman.2015.07.004.

833 [36] Nielsen L, Leithner R. Dynamic Simulation of an Innovative Compressed Air Energy Storage Plant - Detailed Modelling of
834 the Storage Cavern. WSEAS Trans Power Syst 2009;4:253–63.

835 [37] Lim SD, Mazzoleni AP, Park J, Ro PI, Quinlan B. Conceptual design of ocean compressed air energy storage system. Ocean
836 2012 2012:1–8. doi:10.1109/OCEANS.2012.6404909.

837 [38] Barnes FS, Levine JG. Large energy storage systems handbook. Mech Eng Ser 2011:1–260.

838 [39] Luo X, Wang J, Dooner M, Clarke J, Krupke C. Overview of current development in compressed air energy storage
839 technology. Energy Procedia 2014;62:603–11. doi:10.1016/j.egypro.2014.12.423.

840 [40] Nakhamkin M, Schainker RB, Chiruvolu M, Patel M, Byrd S, Marean J. Second Generation of CAES Technology -
841 Performance, Operations, Economics, Renewable Load Management, Green Energy. POWER-GEN Int 2009.

842 [41] Mason JE, Archer CL. Baseload electricity from wind via compressed air energy storage (CAES). Renew Sustain Energy Rev
843 2012;16:1099–109. doi:10.1016/j.rser.2011.11.009.

844 [42] EPRI-DOE. Handbook of Energy Storage for Transmission & Distribution Applications. vol. 2. 2003. doi:1001834.

845 [43] Schulte RH, Critelli N, Holst K, Huff G. Lessons from Iowa: development of a 270 megawatt compressed air energy storage
846 project in Midwest independent system operator. 2012.

847 [44] http://www.worleyparsons.com/Projects/Pages/SenecaCompressedAirEnergyStorage.aspx n.d.

848 [45] http://www.apexcaes.com/project n.d.

849 [46] EPA. apex-matagorda-sob013114.pdf. Rep EPA 2013.

850 [47] Cabe BMJ, Knudsen CDF, Bearden DBM, Horner MCJ, Schaef SRH, Thorne FSP. Techno-economic Performance Evaluation

851   of Compressed Air Energy Storage in the Pacific Northwest. 2013.

852   [48]   Chen L, Zheng T, Mei S, Xuee X, Liu B LQ. Review and prospect of compressed air energy storage system. J Mod Power
853   Syst Clean Energy 2016;4:529–41.

854   [49]   Geth F, Brijs T, Kathan J, Driesen J, Belmans R. An overview of large-scale stationary electricity storage plants in Europe:
855   Current status and new developments. Renew Sustain Energy Rev 2015;52:1212–27. doi:10.1016/j.rser.2015.07.145.

856   [50]   Energy storage: the missing link. Gaelectric Rep n.d. http://www.gaelectric.ie/wpx/wp-content/uploads/2015/09/107715-
857   Galectric-FTI-Booklet.pdf (accessed June 7, 2017).

858   [51]   http://www.gaelectric.ie/energy-storage-projects/ n.d.

859   [52]   Jakiel C, Zunft S, Nowi A. Adiabatic compressed air energy storage plants for efficient peak load power supply from wind
860   energy: the European project AA-CAES. Int J Energy Technol Policy 2007;5:296–306. doi:10.1504/IJETP.2007.014736.

861   [53]   Luo X, Wang J, Dooner M, Clarke J. Overview of current development in electrical energy storage technologies and the
862   application potential in power system operation. Appl Energy 2015;137:511–36. doi:10.1016/j.apenergy.2014.09.081.

863   [54]   Cascetta M, Cau G, Puddu P, Serra F. A study of a packed-bed thermal energy storage device: Test rig, experimental and
864   numerical results. Energy Procedia 2015;81:987–94. doi:10.1016/j.egypro.2015.12.157.

865   [55]   Schumann TEW. Heat transfer: A liquid flowing through a porous prism. J Franklin Inst 1929;208:405–16.
866   doi:10.1016/S0016-0032(29)91186-8.

867   [56]   Marquardt R., Hoffmann S., Pazzi S., Klafki M. ZS. AA-CAES – Opportunities and challenges of advanced adiabatic
868   compressed air energy storage technology as a balancing tool in interconnected grids. 40. Kraftwerkstechnisches Kolloquium
869   2008, Vol. 2, Tech. Univ. Dresden (Ed.)., 2008.

870